Available online at www.sciencedirect.com
ScienceDirect
Journal of Sound and Vibration 299 (2007) 143–163
JOURNAL OF SOUND AND VIBRATION
www.elsevier.com/locate/jsvi

Analytical and numerical results for vibration analysis of multi-stepped and multi-damaged circular arches

Erasmo Viola*, Michele Dilena, Francesco Tornabene

DISTART, Department of Structural Engineering, University of Bologna, Viale Risorgimento 2, I-40136 Bologna, Italy

Received 3 February 2006; received in revised form 4 July 2006; accepted 6 July 2006
Available online 14 September 2006

Abstract

This paper investigates the in-plane linear dynamic behaviour of multi-stepped and multi-damaged circular arches under different boundary conditions. Cracked cross-sections are modelled as massless elastic rotational hinges. In damaged configuration, cracks can be located both at the interface between two adjacent portions as well as inside the portion itself. For each arch portion bounded by two cracks, the differential equations of motion have been established considering axial extension, transverse shear effects and rotatory inertia. The equilibrium equations of arch portions are combined in the coupled fundamental system in terms of radial displacement, tangential displacement and rotation. Analytical and numerical solutions for multi-stepped arches, in undamaged as well as in damaged configurations, are proposed. The analytical solution is based on the Euler characteristic exponent procedure involving the roots of characteristic polynomials, while the numerical method is focused on the Generalized Differential Quadrature (GDQ) method and the Generalized Differential Quadrature Element (GDQE) technique. Numerical results are shown in terms of the first 10 analytical and numerical frequencies of multi-stepped and multi-damaged arches with different boundary conditions. Finally, convergence and stability characteristics of the GDQE procedure are investigated. The convergence rate of the natural frequencies is shown to be very fast and the stability of the numerical procedure is very good.

1. Introduction

The problem of the behaviour of arch structures has attracted considerable attention because of the use of this structural element in a variety of engineering applications. The first studies on this topic date back to the work of Den Hartog [1] and Love [2], but the arch problem is the subject of a number of investigations [3–7] in the present day, too. They involve both theoretical formulations [3–5] and practical applications [6,7].

Following different approaches, many articles involving static and dynamic analyses of arch structures have been published over the past years. Several investigators have carried out finite-element analyses by using various types of curved beam elements. To this end, one may mention Perty and Fleischer [8], Ahmed [9],

*Corresponding author. Tel.: +39 051 209 3510; fax: +39 051 209 3495.
E-mail addresses: erasmo.viola@mail.ing.unibo.it (E. Viola), michele.dilena@mail.ing.unibo.it (M. Dilena), francesco.tornabene@mail.ing.unibo.it (F. Tornabene).

0022-460X/$ - see front matter
doi:10.1016/j.jsv.2006.07.001

Prathap [10], Ashwell and Gallagher [11], Babu and Prathap [12], Cook et al. [13], Dawe [14,15], among others.

An examination of the quality of displacement trial functions in quadratic isoparametric representation of an arch was made by Morley [16], Tessler and Spiridigliozzi [17], Stolarski and Chiang [18]. The boundary-value problem of linear elastic equilibrium for circular arches was formulated in both standard and mixed variational forms by Reddy and Volpi [19]. The existence and the uniqueness of solutions to these equivalent problems were established and the corresponding discrete problems were studied. One of the most accurate elements published so far is the one developed by Friedman and Kosmatka [20]. Their solution may be expressed as trigonometric functions in terms of 18 constants. Numerical examples were performed to demonstrate the element convergence to results obtained from a shear deformable straight beam when the curved beam becomes shallower.

It is worth noting that most of the above literature is dedicated to understanding and overcoming pathologies exhibited by FE models. The highly undesirable situation of numerical deficiency is broadly referred to the shear/membrane locking. Now, it is well known that there are four common approaches to dealing with both membrane and shear locking [21]. It is beyond the aim of this paper to present a comprehensive state of the art of curved beam elements. It should be noted that a review article [22] of more than 10 years ago devoted to the subject of the dynamics of arch-type structures enumerated 407 references.

As far as the research line dealing with analytical solutions is concerned, some contributions have been reported, for example, in Refs. [23–28]. Free and forced in-plane vibrations of circular arches with both variable and uniform cross-sections have been investigated. Exact solutions for the free and forced vibrations of uniform Bernoulli–Euler arches can be found in Refs. [23,24]. The closed-form solution is used for circular arches with stepped cross-sections and is applied to obtain an approximate solution for arches with non-uniform cross-sections in Ref. [25]. Exact and approximate results for the first 10 free vibration frequencies for clamped arches, double-hinged arches and cantilever arches are compared in Ref. [26] for various opening angles. An exact solution of free in-plane vibrations of circular arches having uniform cross-section, by considering axial extension, transverse shear and rotatory inertia effects, is reported in Ref. [27]. An analytical solution for the determination of the natural frequencies of continuous Timoshenko curved beam on Winkler-type elastic foundation is presented in Ref. [28].

Very recently, a closed-form elastic solution for circular arches having uniform cross-section was obtained by Viola et al. [29]. An original procedure for solving the fundamental system of equations was used. The analytical solution is expressed in terms of six unknown constants that may be obtained by imposing constraints at each end of the arch element. A finite-element formulation based on shape functions that satisfy the homogeneous form of the governing system of equation has been developed.

The analysis of curved beams has been the subject of considerable research interest over years. Several varieties of approaches have been employed, depending on the particular problem to solve. However, only a few researchers have studied damaged circular arch structures [5,30,31].

All the studies on the vibration analysis of damaged arches have been confined with structures having only one crack. Moreover, problems concerning the behaviour of stepped structural elements do not take the crack effect into account.

The aim of this paper, thus, is to provide a contribution to the study of free harmonic vibration problem of multi-stepped and multi-damaged arches. Each cracked cross-section is modelled as a massless, elastic rotational hinge [32–36]. This is one of the more convenient techniques for representing the local flexibility introduced by a crack in a structure. In the present paper, each elastic spring connects two arch portions. This elastic hinge model allows discontinuity in rotation, which is proportional to the applied bending moment at the cracked cross-section. Recently, more complex elastic hinge has also been used in vibrating problems involving structural elements [37,38]. For each arch portion bounded by two cracks, the differential equations of motion have been established, considering axial extension, transverse shear effects and rotatory inertia. In fact, the coupled system of second-order differential equations, which represents the equilibrium equations in terms of displacements, contains all the three aspects of the problem of the elastic equilibrium, namely equilibrium equations, strain–displacement and constitutive relations.

When the boundary conditions and the compatibility conditions at the cracked cross-sections of the multi-stepped arch have been imposed, the solution of the investigated problem can be derived.

The present paper generalizes the procedure and the results obtained by Viola et al. [5], for the vibration analysis of a uniform circular arch damaged by only one crack. In this work, we not only have more cracks, but also an arch structure with an arbitrary number of different arch portions. In the multi-stepped arches considered, the damage can be located inside the portions, as well as at cross-sections where two different portions are connected.

An exact analytical method of solution and an approximate numerical one are illustrated. The analytical solution is based on the Euler characteristic exponent procedure involving the roots of characteristic polynomials. The numerical method is focused on the Generalized Differential Quadrature (GDQ) method and Generalized Differential Quadrature Element (GDQE) technique. Only a few Refs. [39–50] about GDQ and GDQE methods will be reported in this paper. More than 200 papers dealing with GDQ and GDQE methods under consideration have been collected by the authors.

2. Statement of the problem

Consider a multi-stepped circular arch, which vibrates freely in its plane, with small oscillations around an unstressed configuration of equilibrium. Suppose that the system is constituted by a sequence of m consecutive portions. Each portion of the arch is characterized by a different thickness, as shown in Fig. 1. Θ is the full amplitude of the considered arch. The kinematics of the (e)th portion, $e = 1, \ldots, m$, is completely defined by assigning the tangential displacement $u^{(e)}(\vartheta, t)$, the normal displacement $v^{(e)}(\vartheta, t)$ and the rotation angle about the binormal axis $\varphi^{(e)}(\vartheta, t)$ of the angular coordinate ϑ at a moment of time t. Taking into account the effect of shear and axial deformations and rotatory inertia, the equations of motion can be written as

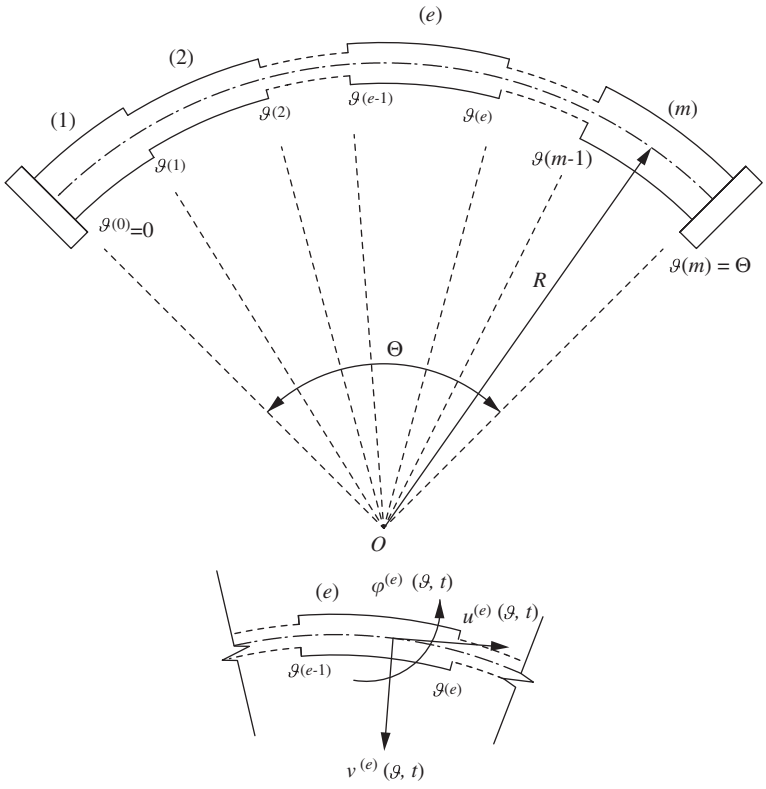

Fig. 1. Multi-stepped circular arch in undamaged configuration.

follows [5,20,29,50]:

$$\frac{1}{R}\frac{\partial N^{(e)}(\vartheta,t)}{\partial\vartheta}-\frac{T^{(e)}(\vartheta,t)}{R}=\rho A^{(e)}\frac{\partial^2 u^{(e)}(\vartheta,t)}{\partial t^2},$$
$$\frac{1}{R}\frac{\partial T^{(e)}(\vartheta,t)}{\partial\vartheta}+\frac{N^{(e)}(\vartheta,t)}{R}=\rho A^{(e)}\frac{\partial^2 v^{(e)}(\vartheta,t)}{\partial t^2},$$
$$\frac{1}{R}\frac{\partial M^{(e)}(\vartheta,t)}{\partial\vartheta}-T^{(e)}(\vartheta,t)=\rho I^{(e)}\frac{\partial^2\varphi^{(e)}(\vartheta,t)}{\partial t^2},\tag{1}$$

for $\vartheta\in(\vartheta^{(e-1)},\vartheta^{(e)})$, $t>0$ and $e=1,\ldots,m$. In the previous equations, $N^{(e)}(\vartheta,t)$, $T^{(e)}(\vartheta,t)$ and $M^{e}(\vartheta,t)$, denote the axial force, the shearing force and the bending moment, respectively, acting on the (e)th portion of the arch. Moreover, R is the radius of the arch, ρ is the mass per unit volume, $A^{(e)}$ and $I^{(e)}$ are the area and the moment of inertia of the cross-section of the arch portion. The internal forces can be expressed by the constitutive relations [5,20,29,50]:

$$N^{(e)}(\vartheta,t)=\frac{EA^{(e)}}{R}\left(\frac{\partial u^{(e)}(\vartheta,t)}{\partial\vartheta}-v^{(e)}(\vartheta,t)\right),$$
$$T^{(e)}(\vartheta,t)=\frac{GA^{(e)}}{R\chi}\left(u^{(e)}(\vartheta,t)+\frac{\partial v^{(e)}(\vartheta,t)}{\partial\vartheta}+R\varphi^{(e)}(\vartheta,t)\right),$$
$$M^{(e)}(\vartheta,t)=\frac{EI^{(e)}}{R}\frac{\partial\varphi^{(e)}(\vartheta,t)}{\partial\vartheta},\tag{2}$$

where E, G are Young's and shear modules, χ is the shear factor.

If the arch is clamped at $\vartheta=0$ and Θ, then the boundary conditions, for $t>0$, take the form:

$$u^{(1)}(0,t)=0,\quad u^{(m)}(\Theta,t)=0,$$
$$v^{(1)}(0,t)=0,\quad v^{(m)}(\Theta,t)=0,$$
$$\varphi^{(1)}(0,t)=0,\quad \varphi^{(m)}(\Theta,t)=0,\tag{3}$$

if the arch is hinged at $\vartheta=0$ and Θ, then the boundary conditions, for $t>0$, can be expressed as,

$$u^{(1)}(0,t)=0,\quad u^{(m)}(\Theta,t)=0,$$
$$v^{(1)}(0,t)=0,\quad v^{(m)}(\Theta,t)=0,$$
$$M^{(1)}(0,t)=0,\quad M^{(m)}(\Theta,t)=0,\tag{4}$$

while if the arch is clamped at $\vartheta=0$ and free at $\vartheta=\Theta$, then the boundary conditions, for $t>0$, assume the following aspect:

$$u^{(1)}(0,t)=0,\quad N^{(m)}(\Theta,t)=0,$$
$$v^{(1)}(0,t)=0,\quad T^{(m)}(\Theta,t)=0,$$
$$\varphi^{(1)}(0,t)=0,\quad M^{(m)}(\Theta,t)=0.\tag{5}$$

Finally, the continuity and the equilibrium conditions between the (e)th and the $(e+1)$th arch portions at $\vartheta=\vartheta^{(e)}$, require that:

$$u^{(e+1)}(\vartheta^{(e)},t)=u^{(e)}(\vartheta^{(e)},t),$$
$$v^{(e+1)}(\vartheta^{(e)},t)=v^{(e)}(\vartheta^{(e)},t),$$
$$\varphi^{(e+1)}(\vartheta^{(e)},t)=\varphi^{(e)}(\vartheta^{(e)},t),$$
$$N^{(e+1)}(\vartheta^{(e)},t)=N^{(e)}(\vartheta^{(e)},t),$$
$$T^{(e+1)}(\vartheta^{(e)},t)=T^{(e)}(\vartheta^{(e)},t),$$
$$M^{(e+1)}(\vartheta^{(e)},t)=M^{(e)}(\vartheta^{(e)},t),\tag{6}$$

for $t>0$ and $e=1,...,m-1$. Substituting the constitutive relations (2) in (1), the equations of motion can be written in terms of displacement components:

$$\frac{EA^{(e)}}{R^2}\frac{\partial}{\partial\vartheta}\left(\frac{\partial u^{(e)}(\vartheta,t)}{\partial\vartheta}-v^{(e)}(\vartheta,t)\right)-\frac{GA^{(e)}}{R^2\chi}\left(u^{(e)}(\vartheta,t)+\frac{\partial v^{(e)}(\vartheta,t)}{\partial\vartheta}+R\varphi^{(e)}(\vartheta,t)\right)=\rho A^{(e)}\frac{\partial^2 u^{(e)}(\vartheta,t)}{\partial t^2},$$

$$\frac{GA^{(e)}}{R^2\chi}\frac{\partial}{\partial\vartheta}\left(u^{(e)}(\vartheta,t)+\frac{\partial v^{(e)}(\vartheta,t)}{\partial\vartheta}+R\varphi^{(e)}(\vartheta,t)\right)+\frac{EA^{(e)}}{R^2}\left(\frac{\partial u^{(e)}(\vartheta,t)}{\partial\vartheta}-v^{(e)}(\vartheta,t)\right)=\rho A^{(e)}\frac{\partial^2 v^{(e)}(\vartheta,t)}{\partial t^2},$$

$$\frac{EI^{(e)}}{R^2}\frac{\partial^2\varphi^{(e)}(\vartheta,t)}{\partial\vartheta^2}-\frac{GA^{(e)}}{R\chi}\left(u^{(e)}(\vartheta,t)+\frac{\partial v^{(e)}(\vartheta,t)}{\partial\vartheta}+R\varphi^{(e)}(\vartheta,t)\right)=\rho I^{(e)}\frac{\partial^2\varphi^{(e)}(\vartheta,t)}{\partial t^2}. \tag{7}$$

The previous expressions show that the small vibrations of the circular stepped arch are governed by a system of three partial differential equations for each portion identified by the angular coordinates $\vartheta^{(e-1)}$ and $\vartheta^{(e)}$, where a coupling takes place between tangential displacement $u^{(e)}(\vartheta,t)$, normal displacement $v^{(e)}(\vartheta,t)$ and rotation $\varphi^{(e)}(\vartheta,t)$.

Suppose now that a crack appears at the cross-section of angular coordinate $\vartheta^{(e)}$ between the (e)th and the $(e+1)$th arch portions, as shown in Fig. 2. Assuming that the crack always remains open during the vibration of the arch, it can be modelled as a massless, rotational elastic spring at the damaged cross-section [34–38]. The stiffness K of the spring can be related in a precise way to the geometry of damage [30].

The equations of motion take the form (7), while the continuity conditions (6) are replaced by:

$$\begin{aligned}
&u^{(e+1)}(\vartheta^{(e)},t)=u^{(e)}(\vartheta^{(e)},t),\\
&v^{(e+1)}(\vartheta^{(e)},t)=v^{e}(\vartheta^{e},t),\\
&K(\varphi^{(e+1)}(\vartheta^{(e)},t)-\varphi^{(e)}(\vartheta^{(e)},t))=M^{(e)}(\vartheta^{(e)},t),\\
&N^{(e+1)}(\vartheta^{(e)},t)=N^{(e)}(\vartheta^{(e)},t),\\
&T^{(e+1)}(\vartheta^{(e)},t)=T^{(e)}(\vartheta^{(e)},t),\\
&M^{(e+1)}(\vartheta^{(e)},t)=M^{(e)}(\vartheta^{(e)},t),
\end{aligned} \tag{8}$$

for $t>0$. If the crack appears at the cross-section of angular coordinate ϑ^{*} of the (e)th arch portion, then the arch portion is split into two parts, as shown in Fig. 3. The corresponding equations of motions (7) can be written separately for the two parts, $(\vartheta^{(e-1)},\vartheta^{*})$ and $(\vartheta^{*},\vartheta^{(e)})$, located on the left and on the right of the crack. The continuity conditions of displacements and internal forces and the discontinuity of the slope of the arch axis at the crack location ϑ^{*} are given by:

$$\begin{aligned}
&u^{(e,2)}(\vartheta^{*},t)=u^{(e,1)}(\vartheta^{*},t),\\
&v^{(e,2)}(\vartheta^{*},t)=v^{(e,1)}(\vartheta^{*},t),\\
&K(\varphi^{(e,2)}(\vartheta^{*},t)-\varphi^{(e,1)}(\vartheta^{*},t))=M^{(e,1)}(\vartheta^{*},t),\\
&N^{(e,2)}(\vartheta^{*},t)=N^{(e,1)}(\vartheta^{*},t),\\
&T^{(e,2)}(\vartheta^{*},t)=T^{(e,1)}(\vartheta^{*},t),\\
&M^{(e,2)}(\vartheta^{*},t)=M^{(e,1)}(\vartheta^{*},t),
\end{aligned} \tag{9}$$

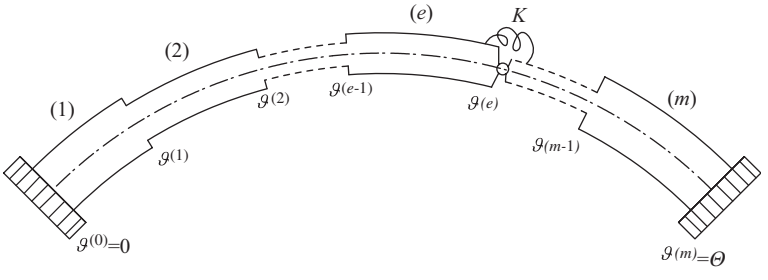

Fig. 2. Multi-stepped circular arch in damaged configuration with a crack located at the interface between two adjacent portions.

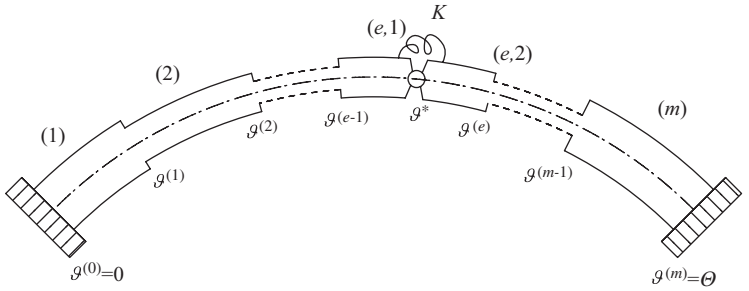

Fig. 3. Multi-stepped circular arch in damaged configuration with a crack internal to e(th) portion.

for $t>0$, where the indices 1, 2 denote the left $(\vartheta^{(e-1)}, \vartheta^*)$ and the right $(\vartheta^*, \vartheta^{(e)})$ parts of the (e)th arch portion, respectively.

Finally, it is easy to extend the study of the free vibration problem to the case of a multi-stepped arch with an arbitrary number of cracks by arranging in a proper set, the boundary conditions (3), (4) or (5), the continuity conditions (6) or (8) between two consecutive portions, the continuity and jump conditions (9) in the presence of one or more cracks internal to the portions.

In the following section, multi-stepped arches in undamaged and damaged configurations will be closely examined.

3. Analytical and numerical solutions

3.1. Exact solution

Consider first the case of a multi-stepped arch in undamaged configuration, that is, in absence of cracks. The governing equations of free vibrations are the coupled system of partial differential equations (7), with the suitable boundary conditions (3)–(5) in the case of clamped–clamped, hinged–hinged or clamped–free ends, respectively, and with the continuity conditions (6). We seek solutions that are harmonic in time and whose frequency is ω; then, in each arch portion, the displacements and the rotation can be written as [5,29,50]:

$$\begin{aligned} u^{(e)}(\vartheta,t) &= U^{(e)}(\vartheta)\cos\omega t,\\ v^{(e)}(\vartheta,t) &= V^{(e)}(\vartheta)\cos\omega t,\\ \varphi^{(e)}(\vartheta,t) &= \Phi^{(e)}(\vartheta)\cos\omega t, \end{aligned} \tag{10}$$

for $\vartheta\in(0,\Theta)$, $t>0$, $e=1,\ldots,m$, where the vibration spatial amplitude values $(U^{(e)}(\vartheta),\ V^{(e)}(\vartheta),\ \Phi^{(e)}(\vartheta))$ satisfy the differential system:

$$\begin{aligned} &\frac{EA^{(e)}}{R^2}\frac{\mathrm{d}^2U^{(e)}(\vartheta)}{\mathrm{d}\vartheta^2}-\frac{GA^{(e)}}{R^2\chi}U^{(e)}(\vartheta)-\left(\frac{EA^{(e)}}{R^2}+\frac{GA^{(e)}}{R^2\chi}\right)\frac{\mathrm{d}V^{(e)}(\vartheta)}{\mathrm{d}\vartheta}-\frac{GA^{(e)}}{R\chi}\Phi^{(e)}(\vartheta)=-\omega^2\rho A^{(e)}U^{(e)}(\vartheta),\\ &\frac{GA^{(e)}}{R^2\chi}\frac{\mathrm{d}^2V^{(e)}(\vartheta)}{\mathrm{d}\vartheta^2}-\frac{EA^{(e)}}{R^2}V^{(e)}(\vartheta)+\left(\frac{EA^{(e)}}{R^2}+\frac{GA^{(e)}}{R^2\chi}\right)\frac{\mathrm{d}U^{(e)}(\vartheta)}{\mathrm{d}\vartheta}+\frac{GA^{(e)}}{R\chi}\frac{\mathrm{d}\Phi^{(e)}(\vartheta)}{\mathrm{d}\vartheta}=-\omega^2\rho A^{(e)}V^{(e)}(\vartheta),\\ &\frac{EI^{(e)}}{R^2}\frac{\mathrm{d}^2\Phi^{(e)}(\vartheta)}{\mathrm{d}\vartheta^2}-\frac{GA^{(e)}}{\chi}\Phi^{(e)}(\vartheta)-\frac{GA^{(e)}}{R\chi}U^{(e)}(\vartheta)-\frac{GA^{(e)}}{R\chi}\frac{\mathrm{d}V^{(e)}(\vartheta)}{\mathrm{d}\vartheta}=-\omega^2\rho I^{(e)}\Phi^{(e)}(\vartheta). \end{aligned} \tag{11}$$

The boundary conditions for the clamped–clamped arch:

$$\begin{aligned} &U^{(1)}(0)=0, \quad U^{(m)}(\Theta)=0,\\ &V^{(1)}(0)=0, \quad V^{(m)}(\Theta)=0,\\ &\Phi^{(1)}(0)=0, \quad \Phi^{(m)}(\Theta)=0, \end{aligned} \tag{12}$$

for the hinged–hinged arch:

$$\begin{aligned} &U^{(1)}(0)=0, \quad U^{(m)}(\Theta)=0,\\ &V^{(1)}(0)=0, \quad V^{(m)}(\Theta)=0,\\ &\frac{\mathrm{d}\Phi^{(1)}(0)}{\mathrm{d}\vartheta}=0, \quad \frac{\mathrm{d}\Phi^{(m)}(\Theta)}{\mathrm{d}\vartheta}=0, \end{aligned} \tag{13}$$

and for the clamped–free:

$$\begin{aligned} &U^{(1)}(0)=0, \quad \frac{\mathrm{d}U^{(m)}(\Theta)}{\mathrm{d}\vartheta}-V^{(m)}(\Theta)=0,\\ &V^{(1)}(0)=0, \quad U^{(m)}(\Theta)+\frac{\mathrm{d}V^{(m)}(\Theta)}{\mathrm{d}\vartheta}+R\Phi^{(m)}(\Theta)=0,\\ &\Phi^{(1)}(0)=0, \quad \frac{\mathrm{d}\Phi^{(m)}(\Theta)}{\mathrm{d}\vartheta}=0, \end{aligned} \tag{14}$$

can be expressed in the forms presented above. Substituting Eq. (10) into Eq. (6), the continuity conditions are expressed as:

$$\begin{aligned} &U^{(e+1)}(\vartheta^{(e)})=U^{(e)}(\vartheta^{(e)}),\\ &V^{(e+1)}(\vartheta^{(e)})=V^{(e)}(\vartheta^{(e)}),\\ &\Phi^{(e+1)}(\vartheta^{(e)})=\Phi^{(e)}(\vartheta^{(e)}),\\ &N^{(e+1)}(\vartheta^{(e)})=N^{(e)}(\vartheta^{(e)}),\\ &T^{(e+1)}(\vartheta^{(e)})=T^{(e)}(\vartheta^{(e)}),\\ &M^{(e+1)}(\vartheta^{(e)})=M^{(e)}(\vartheta^{(e)}), \end{aligned} \tag{15}$$

for $t>0$, $e=1,\ldots,m-1$. Considering the presence of a crack, the continuity conditions (8) and (9) take the form below, respectively:

$$\begin{aligned} &U^{(e+1)}(\vartheta^{(e)})=U^{(e)}(\vartheta^{(e)}),\\ &U^{(e+1)}(\vartheta^{(e)})=V^{(e)}(\vartheta^{(e)}),\\ &K\left(\Phi^{(e+1)}(\vartheta^{(e)})-\Phi^{(e)}(\vartheta^{(e)})\right)=M^{(e)}(\vartheta^{(e)}),\\ &N^{(e+1)}(\vartheta^{(e)})=N^{(e)}(\vartheta^{(e)}),\\ &T^{(e+1)}(\vartheta^{(e)})=T^{(e)}(\vartheta^{(e)}),\\ &M^{(e+1)}(\vartheta^{(e)})=M^{(e)}(\vartheta^{(e)}), \end{aligned} \tag{16}$$

$$\begin{aligned} &U^{(e,2)}(\vartheta^{*})=U^{(e,1)}(\vartheta^{*}),\\ &V^{(e,2)}(\vartheta^{*})=V^{(e,1)}(\vartheta^{*}),\\ &K\left(\Phi^{(e,2)}(\vartheta^{*})-\Phi^{(e,1)}(\vartheta^{*})\right)=M^{(e,1)}(\vartheta^{*}),\\ &N^{(e,2)}(\vartheta^{*})=N^{(e,1)}(\vartheta^{*}),\\ &T^{(e,2)}(\vartheta^{*})=T^{(e,1)}(\vartheta^{*}),\\ &M^{(e,2)}(\vartheta^{*})=M^{(e,1)}(\vartheta^{*}). \end{aligned} \tag{17}$$

The complete primitive $(U^{(e)}(\vartheta),\ V^{(e)}(\vartheta),\ \Phi^{(e)}(\vartheta))$ of system (11) takes the form [5]:

$$\left(U^{(e)}(\vartheta),\ V^{(e)}(\vartheta),\Phi^{(e)}(\vartheta)\right)=\sum_{\alpha=1}^{6}c_{\alpha}^{(e)}\mathbf{w}_{\alpha}^{(e)}\ \exp\left(\lambda_{\alpha}^{(e)}\vartheta\right), \tag{18}$$

for $e = 1, \ldots, m-1$, where $\{c_\alpha^{(e)}\}_{\alpha=1}^{6} = \mathbf{c}^{(e)}$ is a vector of unknown constants which depend on the boundary and continuity conditions. In Eq. (18), $\{\lambda_\alpha^{(e)}, \mathbf{w}_\alpha^{(e)} \equiv (w_{\alpha,1}^{(e)}, w_{\alpha,2}^{(e)}, w_{\alpha,3}^{(e)})\}$ is the α(th) eigenpair of the eigenvalue problem in terms of the ϑ spatial variable, for the (e)th interval of the arch. Applying the Euler characteristic exponent method, we seek solutions for system (11) having the form $\mathbf{w}_\alpha^{(e)} \exp(\lambda_\alpha^{(e)}\vartheta)$.

The six complex numbers $\{\lambda_\alpha^{(e)}\}_{\alpha=1}^{6}$, for a given index e, are the roots of the characteristic polynomials:

$$p^{(e)}(\lambda_\alpha^{(e)}) = d_{0e} + d_{1e}(\lambda_\alpha^{(e)})^2 + d_{2e}(\lambda_\alpha^{(e)})^4 + d_{3e}(\lambda_\alpha^{(e)})^6, \tag{19}$$

where

$$\begin{aligned}
d_{0e} &= EA^{(e)}\frac{GA^{(e)}}{\chi}(A^{(e)}R^2 + I^{(e)})\Omega - \left[EA^{(e)}I^{(e)} + \frac{GA^{(e)}}{\chi}\left(A^{(e)}R^2 + I^{(e)}\right)\right]A^{(e)}\Omega^2 + (A^{(e)})^2 I^{(e)}\Omega^3,\\
d_{1e} &= EA^{(e)}\frac{GA^{(e)}}{\chi}EI^{(e)} - EA^{(e)}\left[\frac{GA^{(e)}}{\chi}\left(A^{(e)}R^2 - I^{(e)}\right) + EA^{(e)}I^{(e)}\right]\Omega + \left(2EA^{(e)} + \frac{GA^{(e)}}{\chi}\right)A^{(e)}I^{(e)}\Omega^2,\\
d_{2e} &= 2EA^{(e)}\frac{GA^{(e)}}{\chi}EI^{(e)} + \left(EA^{(e)} + 2\frac{GA^{(e)}}{\chi}\right)EA^{(e)}I^{(e)}\Omega,\\
d_{3e} &= EA^{(e)}\frac{GA^{(e)}}{\chi}EI^{(e)},
\end{aligned} \tag{20}$$

and $\Omega = \omega^2\rho R^2$. Considering that the $\mathbf{w}_\alpha^{(e)}$ eigenvector, with $\alpha = 1, \ldots, 6$, is proportional to the vector of components:

$$\begin{aligned}
w_1 &= 1,\\
w_2(\lambda_\alpha^{(e)}) &= -\frac{\lambda_\alpha^{(e)}[EA^{(e)}((\lambda_\alpha^{(e)})^2 + 1) + A^{(e)}\Omega]}{A^{(e)}\Omega - EA^{(e)}((\lambda_\alpha^{(e)})^2 + 1)},\\
w_3(\lambda_\alpha^{(e)}) &= \frac{\chi}{GA^{(e)}R}\left[\left(EA^{(e)}(\lambda_\alpha^{(e)})^2 - \frac{GA^{(e)}}{\chi} + A^{(e)}\Omega\right) - \lambda_\alpha^{(e)}\left(EA^{(e)} + \frac{GA^{(e)}}{\chi}\right)w_2(\lambda_\alpha^{(e)})\right],
\end{aligned} \tag{21}$$

the characteristic polynomial can be formed for the eigenvalue problem (11), by imposing that the general solution (18) must satisfy boundary conditions (12), (13) or (14) and the jump conditions (15), (16) or (17). Thus, one obtains a homogeneous linear system in real constants $\mathbf{c} = \{\mathbf{c}^{(e)}\}_{e=1}^{m}$, say, $\mathbf{M}(\omega)\mathbf{c} = \mathbf{0}$, where $\mathbf{M}(\omega)$ is a $6m \times 6m$ matrix depending on ω. Natural cyclic pulsations correspond to those special ω values that set the determinant of $\mathbf{M}(\omega)$ equal to zero. In order to determine the natural pulsations of the arch as roots of the characteristic polynomial $\det \mathbf{M}(\omega)$, a numeric procedure was adopted, the essential steps of which have been explained in Ref. [5]. Finally, for each eigenfrequency value, the vector $\mathbf{c}$ has been evaluated and the corresponding mode shape has been determined.

To conclude this section, suppose now that one or more cracks appear in some cross-sections of the arch. In that case, taking into account Eqs. (8) and (9), it is sufficient to write the proper continuity and jump conditions and repeat the procedure described above.

3.2. GDQE technique review

The GDQ method will be used to discretize the partial space derivatives in the governing equations and in the boundary conditions. The essence of the Differential Quadrature (DQ) method is that the partial or total derivate of a smooth function with respect to a variable is approximated by a weighted sum of function values at all discrete points in the direction involved by the variable under consideration. The GDQ approach was developed by Shu [44] to improve the DQ technique [39,40] for the computation of weighting coefficients. The weighting coefficients are not related to any special problem and only depend on the grid points and the derivate order. In this methodology, an arbitrary grid distribution can be chosen without any limitation.

Thus, the n(th)-order derivative of function $f(\vartheta)$ with respect to ϑ at a grid points ϑ_i, can be approximated by the GDQ approach:

$$\left.\frac{\mathrm{d}^n f(\vartheta)}{\mathrm{d}\vartheta^n}\right|_{\vartheta=\vartheta_i} \cong \sum_{j=1}^{\mathscr{N}} \beta_{ij}^{(n)} f(\vartheta_j), \quad i = 1, 2, \ldots, \mathscr{N}, \tag{22}$$

where $\beta_{ij}^{(n)}$ are the weighting coefficients of the n(th)-order derivative at the i(th) sampling points along the domain. $\mathscr{N}$ is the total number of the sampling points of the grid distribution and $f(\vartheta_j)$ are the function values at grid points.

The weighting coefficients can be determined by the interpolation rule chosen. For the cases treated in the present paper, Lagrange polynomial functions have been adopted.

The Lagrange interpolating polynomials can be defined by the formula:

$$p_j(\vartheta) = \frac{\mathscr{L}(\vartheta)}{(\vartheta - \vartheta_j)\mathscr{L}^{(1)}(\vartheta_j)}, \quad j = 1, \ldots, \mathscr{N}, \tag{23}$$

where

$$\mathscr{L}(\vartheta) = \prod_{i=1}^{N}(\vartheta - \vartheta_i), \quad \mathscr{L}^{(1)}(\vartheta_j) = \prod_{i=1, i\neq j}^{N}(\vartheta_j - \vartheta_i). \tag{24}$$

With this choice, some simple recursive formulas are available for calculating weighting coefficients [44]. For the first-order derivative, we have:

$$\beta_{ij}^{(1)} = \frac{\mathscr{L}^{(1)}(\vartheta_i)}{(\vartheta_i - \vartheta_j)\mathscr{L}^{(1)}(\vartheta_j)}, \quad i,j = 1, 2, \ldots, \mathscr{N}, \quad i \neq j, \tag{25}$$

$$\sum_{j=1}^{N} \beta_{ij}^{(1)} = 0 \Rightarrow \beta_{ii}^{(1)} = -\sum_{j=1, j\neq i}^{N} \beta_{ij}^{(1)}, \quad i,j = 1, 2, ..., \mathscr{N}, \ i = j. \tag{26}$$

For higher-order derivatives, one gets iteratively:

$$\beta_{ij}^{(n)} = n\left(\beta_{ii}^{(n-1)}\beta_{ij}^{(1)} - \frac{\beta_{ij}^{(n-1)}}{\vartheta_i - \vartheta_j}\right), \quad i \neq j, \quad n = 2, 3, \ldots, \mathscr{N} - 1, \quad i,j = 1, 2, \ldots, \mathscr{N}, \tag{27}$$

$$\sum_{j=1}^{N} \beta_{ij}^{(n)} = 0 \Rightarrow \beta_{ii}^{(n)} = -\sum_{j=1, j\neq i}^{N} \beta_{ij}^{(n)}, \quad i = j, \quad n = 2, 3, \ldots, \mathscr{N} - 1, \quad i,j = 1, 2, \ldots, \mathscr{N}. \tag{28}$$

The GDQ method may be used as an efficient numerical tool for solving problems which have every form of discontinuity in geometry, material or loading at any point of the problem domain in the form of sub-domain elements. In fact, when any form of discontinuity appears at any domain point, use of the domain decomposition technique is needed to solve the problem by means of the GDQ method. As with the finite-element method , the domain of a problem is first separated into a certain number of sub-domains or elements. This operation is called domain decomposition technique. Civan and Sliepcevich [48,49] introduced the domain decomposition technique with DQ method for the first time. Then, the GDQ discretization is carried out on each sub-domain. The use of the GDQ method on each sub-domain, together with the use of the domain decomposition technique, is named GDQE technique [45].

Thus, the governing differential or partial differential equations defined on each element (11), the transition conditions on inter-element boundaries (15), (16) or (17) and the boundary conditions on the domain boundary (12)–(14) are in discrete form after GDQE application. Assembling all the discrete fundamental equations, the overall algebraic system can be obtained and used to solve the problem.

The governing equations of each sub-domain are the same as those of a single domain obtained before. In addition to the external boundary conditions, the kinematical and physical compatibility should be satisfied at the common cross-section of the two adjacent sub-domains (15)–(17). The kinematical compatibility

conditions include the continuity of axial and radial displacements as well as rotation. The physical compatibility conditions can only be the three continuity conditions for the bending moment, shear force and axial force.

For the numerical computations presented in this paper, the coordinates of grid points are chosen as

$$\vartheta_i^{(e)} = \frac{1-\cos(i-1)/(N^{(e)}-1)\pi)}{2}(\vartheta^{(e)}-\vartheta^{(e-1)}), \quad i=1,\ldots,N^{(e)}, \tag{29}$$

where $(\vartheta^{(e)}-\vartheta^{(e-1)})$ and $\mathcal{N}^{(e)}$ are the full amplitude of the e(th) arch portion and the total number of sampling points used to discretize it, respectively. In this work, the same number of sampling points $\mathcal{N}^{(e)}=\mathcal{N}$ for each sub-domain 'e' is used. With Lagrange interpolating polynomials (23), the Chebyshev–Gauss–Lobatto sampling point rule (29) proves efficient for numerical reasons [44], so that for such a collocation the approximation error of dependent variables decreases as the number of nodes increases.

3.3. Numerical implementation

The numerical operations illustrated above enable one to write the equations of motion in discrete form, transforming every space derivative into a weighted sum of node values of dependent variables applying the GDQ procedure. Each equation is valid in a single sampling point belonging to one of the arch portions. For the generic arch portion 'e' and its interior sampling points, $i=2,3,\ldots,\mathcal{N}^{(e)}-1$, the governing Eqs. (11) can be discretized as follows:

$$\begin{aligned}
&\frac{EA_i^{(e)}}{R^2}\sum_{j=1}^{\mathcal{N}^{(e)}}\beta_{ij}^{(2)(e)}U_j^{(e)} - \frac{GA_i^{(e)}}{R^2\chi}\,U_i^{(e)} - \left(\frac{EA_i^{(e)}}{R^2}+\frac{GA_i^{(e)}}{R^2\chi}\right)\sum_{j=1}^{\mathcal{N}^{(e)}}\beta_{ij}^{(1)(e)}V_j^{(e)} - \frac{GA_i^{(e)}}{R\chi}\,\Phi_i^{(e)} = -\omega^2\rho A_i^{(e)}U_i^{(e)},\\
&\frac{GA_i^{(e)}}{R^2\chi}\sum_{j=1}^{\mathcal{N}^{(e)}}\beta_{ij}^{(2)(e)}V_j^{(e)} - \frac{EA_i^{(e)}}{R^2}\,V_i^{(e)} + \left(\frac{EA_i^{(e)}}{R^2}+\frac{GA_i^{(e)}}{R^2\chi}\right)\sum_{j=1}^{\mathcal{N}^{(e)}}\beta_{ij}^{(1)(e)}U_j^{(e)} + \frac{GA_i^{(e)}}{R\chi}\sum_{j=1}^{N^{(e)}}\beta_{ij}^{(1)(e)}\Phi_j^{(e)} = -\omega^2\rho A_i^{(e)}V_i^{(e)},\\
&\frac{EI_i^{(e)}}{R^2}\sum_{j=1}^{\mathcal{N}^{(e)}}\beta_{ij}^{(2)(e)}\Phi_j^{(e)} - \frac{GA_i^{(e)}}{\chi}\,\Phi_i^{(e)} - \frac{GA_i^{(e)}}{R\chi}\,U_i^{(e)} - \frac{GA_i^{(e)}}{R\chi}\sum_{j=1}^{\mathcal{N}^{(e)}}\beta_{ij}^{(1)(e)}V_j^{(e)} = -\omega^2\rho I_i^{(e)}\Phi_i^{(e)}.
\end{aligned} \tag{30}$$

Applying the GDQ methodology, the discretized forms of the boundary conditions are given below:

- Clamped edge boundary condition:

$$U_i^{(e)}=0,\ V_i^{(e)}=0,\ \Phi_i^{(e)}=0 \quad \text{for } i=1,\ e=1 \quad \text{or } i=\mathcal{N}^{(e)},\ e=m. \tag{31}$$

- Hinged edge boundary condition:

$$U_i^{(e)}=0,\ V_i^{(e)}=0,\ \sum_{j=1}^{\mathcal{N}^{(e)}}\beta_{ij}^{(1)(e)}\Phi_j^{(e)}=0 \quad \text{for } i=1,\ e=1 \quad \text{or } i=\mathcal{N}^{(e)},\ e=m. \tag{32}$$

- Free edge boundary condition:

$$\begin{aligned}
&\sum_{j=1}^{\mathcal{N}^{(e)}}\beta_{ij}^{(1)(e)}U_j^{(e)} - V_i^{(e)} = 0,\ \sum_{j=1}^{\mathcal{N}^{(e)}}\beta_{ij}^{(1)(e)}V_j^{(e)} + U_i^{(e)} + R\Phi_i^{(e)} = 0,\ \sum_{j=1}^{\mathcal{N}^{(e)}}\beta_{ij}^{(1)(e)}\Phi_j^{(e)} = 0\\
&\text{for } i=1,\ e=1 \quad \text{or } i=\mathcal{N}^{(e)},\ e=m.
\end{aligned} \tag{33}$$

It should be noted that in correspondence of each discontinuity regarding the properties of the arch, jump conditions (15) must be imposed by means of the GDQ method:

$$
\begin{aligned}
&U_1^{(e+1)} = U_{N^{(e)}}^{(e)}, \quad \frac{EA_1^{(e+1)}}{R}\left(\sum_{j=1}^{N^{(e+1)}} \beta_{1j}^{(1)(e+1)} U_j^{(e+1)} - V_1^{(e+1)}\right) = \frac{EA_{N^{(e)}}^{(e)}}{R}\left(\sum_{j=1}^{N^{(e)}} \beta_{N^{(e)}j}^{(1)(e)} U_j^{(e)} - V_{N^{(e)}}^{(e)}\right),\\
&V_1^{(e+1)} = V_{N^{(e)}}^{(e)}, \quad \frac{GA_1^{(e+1)}}{R\chi}\left(\sum_{j=1}^{N^{(e+1)}} \beta_{1j}^{(1)(e+1)} V_j^{(e+1)} + U_1^{(e+1)} + R\Phi_1^{(e+1)}\right)\\
&\qquad = \frac{GA_{N^{(e)}}^{(e)}}{R\chi}\left(\sum_{j=1}^{N^{(e)}} \beta_{N^{(e)}j}^{(1)(e)} V_j^{(e)} + U_{N^{(e)}}^{(e)} + R\Phi_{N^{(e)}}^{(e)}\right),\\
&\Phi_1^{(e+1)} = \Phi_{N^{(e)}}^{(e)}, \quad \frac{EI_1^{(e+1)}}{R}\sum_{j=1}^{N^{(e+1)}} \beta_{1j}^{(1)(e+1)} \Phi_j^{(e+1)} = \frac{EI_{N^{(e)}}^{(e)}}{R}\sum_{j=1}^{N^{(e)}} \beta_{N^{(e)}j}^{(1)(e)} \Phi_j^{(e)}.
\end{aligned} \tag{34}
$$

In presence of crack, the jump conditions (16) or (17) can be written in discrete form as

$$
\begin{aligned}
&U_1^{(e+1)} = U_{\mathcal{N}^{(e)}}^{(e)}, \quad \frac{EA_1^{(e+1)}}{R}\left(\sum_{j=1}^{\mathcal{N}^{(e+1)}} \beta_{1j}^{(1)(e+1)} U_j^{(e+1)} - V_1^{(e+1)}\right) = \frac{EA_{\mathcal{N}^{(e)}}^{(e)}}{R}\left(\sum_{j=1}^{\mathcal{N}^{(e)}} \beta_{\mathcal{N}^{(e)}j}^{(1)(e)} U_j^{(e)} - V_{\mathcal{N}^{(e)}}^{(e)}\right),\\
&V_1^{(e+1)} = V_{\mathcal{N}^{(e)}}^{(e)}, \quad \frac{GA_1^{(e+1)}}{R\chi}\left(\sum_{j=1}^{\mathcal{N}^{(e+1)}} \beta_{1j}^{(1)(e+1)} V_j^{(e+1)} + U_1^{(e+1)} + R\Phi_1^{(e+1)}\right)\\
&\qquad = \frac{GA_{\mathcal{N}^{(e)}}^{(e)}}{R\chi}\left(\sum_{j=1}^{\mathcal{N}^{(e)}} \beta_{\mathcal{N}^{(e)}j}^{(1)(e)} V_j^{(e)} + U_{\mathcal{N}^{(e)}}^{(e)} + R\Phi_{\mathcal{N}^{(e)}}^{(e)}\right),\\
&K(\Phi_1^{(e+1)} - \Phi_{\mathcal{N}^{(e)}}^{(e)}) = \frac{EI_{\mathcal{N}^{(e)}}^{(e)}}{R}\sum_{j=1}^{\mathcal{N}^{(e)}} \beta_{\mathcal{N}^{(e)}j}^{(1)(e)} \Phi_j^{(e)}, \quad \frac{EI_1^{(e+1)}}{R}\sum_{j=1}^{\mathcal{N}^{(e+1)}} \beta_{1j}^{(1)(e+1)} \Phi_j^{(e+1)} = \frac{EI_{\mathcal{N}^{(e)}}^{(e)}}{R}\sum_{j=1}^{\mathcal{N}^{(e)}} \beta_{\mathcal{N}^{(e)}j}^{(1)(e)} \Phi_j^{(e)}.
\end{aligned} \tag{35}
$$

Applying the DQ procedure, the whole system of differential equations can be discretized, and the global assembling leads to the following set of linear algebraic equations:

$$
\left[\begin{array}{c|c} \mathbf{K}_{bb} & \mathbf{K}_{bd} \\ \hline \mathbf{K}_{db} & \mathbf{K}_{dd} \end{array}\right]\left[\begin{array}{c} \boldsymbol{\delta}_b \\ \hline \boldsymbol{\delta}_d \end{array}\right] = \omega^2 \left[\begin{array}{c|c} \mathbf{0} & \mathbf{0} \\ \hline \mathbf{0} & \mathbf{M}_{dd} \end{array}\right]\left[\begin{array}{c} \boldsymbol{\delta}_b \\ \hline \boldsymbol{\delta}_d \end{array}\right] \tag{36}
$$

In the above matrices and vector, the partitioning is set forth by subscripts b and d, referring to the system degrees of freedom and standing for *boundary* and *domain*, respectively. In order to make the computation more efficient, kinematic condensation of non-domain degrees of freedom is performed:

$$
(\mathbf{K}_{dd} - \mathbf{K}_{db}(\mathbf{K}_{bb})^{-1}\mathbf{K}_{bd})\boldsymbol{\delta}_d = \omega^2 \mathbf{M}_{dd}\boldsymbol{\delta}_d. \tag{37}
$$

The natural frequencies of the structure considered can be determined by making the following determinant equal zero:

$$
\left|(\mathbf{K}_{dd} - \mathbf{K}_{db}(\mathbf{K}_{bb})^{-1}\mathbf{K}_{bd}) - \omega^2 \mathbf{M}_{dd}\right| = 0. \tag{38}
$$

4. Numerical applications

Based on the above derivations, in the present paragraph some results and considerations about the free vibration problem of multi-stepped circular arches in undamaged and damaged configurations with different boundary conditions are presented. The analysis has been carried out by means of analytical and numerical procedures illustrated above in order to validate the reliability of the numerical approach, when a large number of natural frequencies need to be evaluated, and also to emphasize how the frequencies of the

Table 1
Physical parameters used in the analysis of free vibrations of the stepped arches being considered

Parameter	Value
Density of mass ρ	$7850\,\mathrm{kg/m^3}$
Young's modulus E	$2.06\times10^{11}\,\mathrm{Pa}$
Poisson coefficient ν	0.3
Shear factor χ	1.2

Table 2
Comparison between analytical and numerical frequencies for a three-stepped circular arch in undamaged configuration with radius $R=1\,m$, width $b=0.045\,m$, different constant thicknesses $h^{(1)}=0.020\,m$, $h^{(2)}=0.015\,m$, $h^{(3)}=0.020\,m$ and sweep angles $\vartheta^{(1)}-\vartheta^{(0)}=30^\circ$, $\vartheta^{(2)}-\vartheta^{(1)}=60^\circ$, $\vartheta^{(3)}-\vartheta^{(2)}=30^\circ$

Mode order	Hinged–hinged			Clamped–clamped		
	Analytical (Hz)	GDQE (Hz)	Error (%)	Analytical (Hz)	GDQE (Hz)	Error (%)
1	27.564	27.564	0.000	49.535	49.535	0.000
2	74.838	74.838	0.000	99.224	99.224	0.000
3	140.321	140.321	0.000	178.742	178.742	0.000
4	215.215	215.215	0.000	261.989	261.989	0.000
5	313.167	313.167	0.000	366.855	366.855	0.000
6	432.367	432.367	0.000	485.004	485.004	0.000
7	576.539	576.539	0.000	646.009	646.009	0.000
8	698.877	698.879	0.000	732.315	732.321	0.001
9	823.817	823.815	0.000	865.512	865.512	0.000
10	882.598	882.603	0.001	969.683	969.694	0.001

Material properties are reported in Table 1. Collocation adopted: $\mathcal{N}^{(e)}=21$ for each of the three portions.

Table 3
Comparison between analytical and numerical frequencies for a three-stepped circular arch in damaged configuration with one crack and with the same geometrical and mechanical proprieties as the arch considered in Table 2

Mode order	Hinged–hinged			Clamped–clamped		
	Analytical (Hz)	GDQE (Hz)	Error (%)	Analytical (Hz)	GDQE (Hz)	Error (%)
1	27.564	27.564	0.000	49.535	49.535	0.000
2	74.397	74.397	0.000	98.603	98.603	0.000
3	140.321	140.321	0.000	178.742	178.742	0.000
4	214.005	214.005	0.000	260.529	260.529	0.000
5	313.167	313.167	0.000	366.855	366.855	0.000
6	429.709	429.709	0.000	482.111	482.111	0.000
7	576.539	576.539	0.000	646.009	646.009	0.000
8	695.638	695.641	0.000	730.251	730.257	0.001
9	822.885	822.883	0.000	862.631	862.631	0.000
10	882.598	882.603	0.001	969.683	969.694	0.001

Angular coordinate of the damage: $\vartheta^*=60^\circ$. Stiffness of the spring: $K=217.31\,\mathrm{kN\,m}$. Collocation adopted: $\mathcal{N}^{(e)}=21$ for each of the four portions.

multi-stepped circular arches vary when one or more cracks, with different damage severity, appear. The mechanical characteristics for the considered arches are listed in Table 1. Various types of rectangular cross-section stepped arches, with constant width $b=0.045\,m$ and constant radius $R=1\,m$, are considered.

Tables 2–5 show the first 10 eigenfrequencies, in Hz, for a three-stepped arch having the same geometrical characteristics and different damage configurations with hinged–hinged and clamped–clamped boundary

Table 4
Comparison between analytical and numerical frequencies for a three-stepped circular arch in damaged configuration with one crack and with the same geometrical and mechanical proprieties as the arch considered in Table 2

Mode order	Hinged–hinged			Clamped–clamped		
	Analytical (Hz)	GDQE (Hz)	Error (%)	Analytical (Hz)	GDQE (Hz)	Error (%)
1	27.564	27.564	0.000	49.535	49.535	0.000
2	73.023	73.023	0.000	96.683	96.683	0.000
3	140.321	140.321	0.000	178.742	178.742	0.000
4	210.374	210.374	0.000	256.179	256.179	0.000
5	313.167	313.167	0.000	366.855	366.855	0.000
6	422.035	422.035	0.000	473.838	473.838	0.000
7	576.539	576.539	0.000	646.009	646.009	0.000
8	686.489	686.491	0.000	724.243	724.249	0.001
9	820.419	820.417	0.000	854.967	854.967	0.000
10	882.598	882.603	0.001	969.683	969.694	0.001

Angular coordinate of the damage: $\vartheta^* = 60^\circ$. Stiffness of the spring: $K = 49.62\,\mathrm{kN\,m}$. Collocation adopted: $\mathcal{N}^{(e)} = 21$ for each of the four portions.

Table 5
Comparison between analytical and numerical frequencies for a three-stepped circular arch in damaged configuration with two cracks and with the same geometrical and mechanical proprieties as the arch considered in Table 2

Mode order	Hinged–hinged			Clamped–clamped		
	Analytical (Hz)	GDQE (Hz)	Error (%)	Analytical (Hz)	GDQE (Hz)	Error (%)
1	26.647	26.647	0.000	48.885	48.885	0.000
2	71.170	71.170	0.000	93.936	93.936	0.000
3	139.821	139.821	0.000	176.359	176.359	0.000
4	209.457	209.457	0.000	256.179	256.179	0.000
5	304.740	304.740	0.000	361.323	361.323	0.000
6	410.976	410.976	0.000	460.399	460.399	0.000
7	571.880	571.880	0.000	634.036	634.036	0.000
8	685.968	685.970	0.000	724.227	724.233	0.001
9	819.677	819.675	0.000	850.859	850.859	0.000
10	865.942	865.947	0.001	963.026	963.035	0.001

Angular coordinates of the damages: $\vartheta^{(1^*)} = 30^\circ$, $\vartheta^{(2^*)} = 60^\circ$. Stiffness of the springs: $K = 49.62\,\mathrm{kN\,m}$. Collocation adopted: $\mathcal{N}^{(e)} = 21$ for each of the four portions.

conditions. The two arch portions near the ends are characterized by the same thickness, $h^{(1)} = h^{(3)} = 0.020\,m$, and the same sweep angle, $\vartheta^{(1)} - \vartheta^{(0)} = \vartheta^{(3)} - \vartheta^{(2)} = 30^\circ$, while the middle one has the thickness $h^{(2)} = 0.015\,m$ and the sweep angle $\vartheta^{(2)} - \vartheta^{(1)} = 60^\circ$. The full amplitude of the symmetric arch considered is $\Theta = 120^\circ$.

In particular, Table 2 presents the results for the undamaged arch, while Tables 3 and 4 show the comparison of the frequencies when only one crack of increasing intensity appears at the middle cross-section. The stiffness of the rotational spring can be expressed in terms of the crack depth in the following form:

$$K = \frac{EI^D}{EI - EI^D}\frac{EI}{R\Delta\vartheta}, \tag{39}$$

where EI^D is the bending stiffness of the notched cross-section and its length can be approximated by the relation $R\Delta\vartheta = h/\alpha$, with $\alpha \cong 2$ [30]. In the applications crack depth equal to $d = 5.0\,mm$ in Table 3, and equal to $d = 7.5\,mm$ in Table 4, have been considered. The corresponding stiffness values are $K = 217.31$ and $49.62\,\mathrm{kNm}$, respectively. Finally, in Table 5 the frequencies of the same arch with two cracks having equal

severity of damage $K = 49.62\,\mathrm{kNm}$, one in the middle cross-section, and the other at the interface between the first two adjacent portions, are reported.

For all the cases examined, it is evident that the GDQE technique produces coincident results when compared with the analytical technique, using only a few sampling points in each sub-domain. The same number of grid points $\mathscr{N}^{(e)} = \mathscr{N} = 21$ is considered in each portion. In particular, Tables 1–7 present well-converging numerical results obtained with the GDQE approach.

Concerning the influence of damages on the dynamic parameters of the system, it is known that, in general, the frequency variations increase with the damage severity, in other words when the elastic stiffness K decreases. However, if the crack is located in a zero sensitivity point for a given mode order, the corresponding frequency does not change, see for instance Tables 3 and 4. The zero sensitivity points are those points at which bending modal shape is equal to zero.

In Tables 6 and 7, the first 10 eigenfrequencies for a three-stepped arch having clamped–free boundary conditions are shown. The three arch portions are characterized by the thicknesses $h^{(1)} = 0.030\,m$, $h^{(2)} = 0.025\,m$, $h^{(3)} = 0.015\,m$ and the sweep angles, $\vartheta^{(1)} - \vartheta^{(0)} = 20^\circ$, $\vartheta^{(2)} - \vartheta^{(1)} = 20^\circ$, $\vartheta^{(3)} - \vartheta^{(2)} = 30^\circ$, respectively. In Table 6 we have considered an arch in undamaged and damaged configuration with a crack at the interface between the first two adjacent portions and $K = 49.62\,\mathrm{kN\,m}$. Moreover, in Table 7 we have added another crack of the same severity in the middle of the second portion. The results are always in good agreement and the previous considerations can be easily extended. Furthermore, in order to verify the reliability and the accuracy of the numerical procedure, Table 8 presents a comparison between the analytical results presented by Tufekci and Ozdemirci [51] and the GDQE results obtained considering the same number of grid points $\mathscr{N}^{(e)} = \mathscr{N} = 21$ for each portion. The GDQE technique produces results in agreement with the analytical technique [51] for all the cases analysed. It is worth noting that the accuracy of numerical solution depends on the number of sampling points used to discretize each portion. In fact, increasing the number of sampling points $\mathscr{N}^{(e)}$, the numerical solution converges to the analytical solution [51], as can be seen in Table 9. Furthermore, the converging rate and the accuracy stability of some natural frequencies for multi-stepped and multi-damaged arches are shown in Figs. 4–10. Well converging results for the first 10 frequencies can be obtained using $\mathscr{N}^{(e)} = \mathscr{N} = 21$ for each portion. It is shown that the accuracy of the numerical solution stays steady with increasing $\mathscr{N}$ and does not decrease due to the numerical instabilities even if $\mathscr{N}$ becomes too large. For all the cases treated, the GDQE technique is stable if the number of grid points increases. As shown in all the figures under consideration, to obtain accurate results for the higher frequencies,

Table 6
Comparison between analytical and numerical frequencies for a three-stepped circular arch in undamaged and damaged configurations with centroidal axis radius $R = 1\,m$, width $b = 0.045\,m$, different constant thicknesses $h^{(1)} = 0.030\,m$, $h^{(2)} = 0.025\,m$, $h^{(3)} = 0.015\,m$ and sweep angles, $\vartheta^{(1)} - \vartheta^{(0)} = 20^\circ$, $\vartheta^{(2)} - \vartheta^{(1)} = 20^\circ$, $\vartheta^{(3)} - \vartheta^{(2)} = 30^\circ$

Mode order	Clamped–free					
	Undamaged			One damage		
	Analytical (Hz)	GDQE (Hz)	Error (%)	Analytical (Hz)	GDQE (Hz)	Error (%)
1	20.433	20.433	0.000	17.342	17.342	0.000
2	67.978	67.978	0.000	67.878	67.878	0.000
3	195.761	195.761	0.000	175.919	175.919	0.000
4	372.498	372.498	0.000	340.394	340.394	0.000
5	643.913	643.913	0.000	625.109	625.109	0.000
6	928.625	928.625	0.000	925.873	925.873	0.000
7	1312.164	1312.164	0.000	1199.618	1199.618	0.000
8	1478.623	1478.623	0.000	1478.101	1478.101	0.000
9	1740.342	1740.342	0.000	1637.069	1637.069	0.000
10	2262.455	2262.455	0.000	2190.763	2190.763	0.000

Angular coordinates of the damage: $\vartheta^* = 20^\circ$. Stiffness of the spring: $K = 49.62\,\mathrm{kN\,m}$. The material properties are reported in Table 1. Collocation adopted: $\mathscr{N}^{(e)} = 21$ for each portion.

Table 7
Comparison between analytical and numerical frequencies for a three-stepped circular arch in undamaged and damaged configurations with two cracks and with the same geometrical and mechanical properties as the arch considered in Table 6

Mode order	Clamped–free					
	Undamaged			Two damages		
	Analytical (Hz)	GDQE (Hz)	Error (%)	Analytical (Hz)	GDQE (Hz)	Error (%)
1	20.433	20.433	0.000	16.274	16.274	0.000
2	67.978	67.978	0.000	65.585	65.585	0.000
3	195.761	195.761	0.000	165.932	165.932	0.000
4	372.498	372.498	0.000	330.708	330.708	0.000
5	643.913	643.913	0.000	532.080	532.080	0.000
6	928.625	928.625	0.000	900.476	900.476	0.000
7	1312.164	1312.164	0.000	1130.762	1130.762	0.000
8	1478.623	1478.623	0.000	1475.961	1475.961	0.000
9	1740.342	1740.342	0.000	1575.733	1575.733	0.000
10	2262.455	2262.455	0.000	2189.364	2189.364	0.000

Angular coordinates of the damages: $\vartheta^{(1^*)} = 20^\circ$, $\vartheta^{(2^*)} = 30^\circ$. Stiffness of the springs: $K = 49.62\,\mathrm{kN\,m}$. Collocation adopted: $\mathcal{N}^{(e)} = 21$ for each portion.

Table 8
Comparison between analytical [51] and numerical frequencies for two-stepped circular arches in undamaged configuration

Clamped–free (Hz)		$\phi_T = \Theta = 120^\circ$			$\phi_T = \Theta = 180^\circ$		
		Analytical [51]	GDQE	Error (%)	Analytical [51]	GDQE	Error (%)
$\psi/\phi_T = -0.2$	1	105.78	105.78	0.00	52.29	52.29	0.00
	2	388.71	388.71	0.00	147.89	147.89	0.00
	3	1223.03	1223.03	0.00	485.49	485.49	0.00
	4	2522.58	2522.58	0.00	1073.31	1073.31	0.00
	5	4071.74	4071.74	0.00	1825.23	1825.23	0.00
	6	5090.80	5090.80	0.00	2735.94	2735.94	0.00
$\psi/\phi_T = 0$	1	113.80	113.80	0.00	56.57	56.57	0.00
	2	405.31	405.31	0.00	155.10	155.10	0.00
	3	1276.94	1276.94	0.00	504.88	504.89	0.00
	4	2557.02	2557.01	0.00	1087.61	1087.61	0.00
	5	4159.28	4159.28	0.00	1892.28	1892.28	0.00
	6	5223.89	5223.89	0.00	2839.25	2839.25	0.00
$\psi/\phi_T = 0.2$	1	113.53	113.53	0.00	56.28	56.28	0.00
	2	447.71	447.71	0.00	171.75	171.75	0.00
	3	1312.76	1312.76	0.00	521.28	521.28	0.00
	4	2652.00	2652.00	0.00	1129.44	1129.44	0.00
	5	4341.77	4341.76	0.00	1986.86	1986.86	0.00
	6	5230.66	5230.66	0.00	2963.95	2963.95	0.00

Material and geometric properties of the above two-stepped arches are illustrated in Ref. [51]. Collocation adopted: $\mathcal{N}^{(e)} = 21$ for each portion.

the number of sampling points must not be too large. Moreover, Figs. 4–10 show that the converging rate of the numerical solutions also depends on the boundary conditions. Based on the reliable results presented in this paper, the numerical approach can be used to solve the problem of multi-stepped and multi-damaged arches in an accurate manner.

Table 9
Comparison between analytical [51] and numerical frequencies for two-stepped circular arches in undamaged configuration for different grid distributions $\mathcal{N}^{(e)}$ in each portion

Clamped–free		Frequencies (Hz)						
$\phi_T = \Theta = 120^\circ$		Analytical [51]	GDQE $\mathcal{N}^{(e)} = 7$	GDQE $\mathcal{N}^{(e)} = 9$	GDQE $\mathcal{N}^{(e)} = 11$	GDQE $\mathcal{N}^{(e)} = 13$	GDQE $\mathcal{N}^{(e)} = 15$	GDQE $\mathcal{N}^{(e)} = 17$
$\psi/\phi_T = -0.2$	1	105.78	107.67	105.77	105.78	105.78	105.78	105.78
	2	388.71	389.98	388.65	388.71	388.71	388.71	388.71
	3	1223.03	1198.45	1223.84	1223.01	1223.03	1223.03	1223.03
	4	2522.58	2417.85	2549.38	2520.98	2522.64	2522.58	2522.58
	5	4071.74	4071.37	4141.89	4065.92	4072.10	4071.73	4071.74
	6	5090.80	5095.46	5124.46	5087.93	5091.01	5090.80	5090.80
$\psi/\phi_T = 0$	1	113.80	114.12	113.80	113.80	113.80	113.80	113.80
	2	405.31	406.78	405.32	405.31	405.31	405.31	405.31
	3	1276.94	1285.46	1276.69	1276.94	1276.94	1276.94	1276.94
	4	2557.01	2547.67	2557.16	2557.01	2557.01	2557.01	2557.01
	5	4159.28	4068.87	4172.19	4158.68	4159.29	4159.28	4159.28
	6	5223.89	5172.37	5236.89	5223.17	5223.92	5223.89	5223.89
$\psi/\phi_T = 0.2$	1	113.53	113.62	113.53	113.53	113.53	113.53	113.53
	2	447.71	452.57	447.64	447.71	447.71	447.71	447.71
	3	1312.76	1324.89	1312.21	1312.77	1312.76	1312.76	1312.76
	4	2652.00	2656.72	2657.71	2651.75	2652.01	2652.00	2652.00
	5	4341.76	4356.95	4358.27	4340.71	4341.81	4341.76	4341.76
	6	5230.66	5454.61	5251.56	5229.40	5230.77	5230.66	5230.66

Material and geometric properties of the above two-stepped arches are illustrated in Ref. [51].

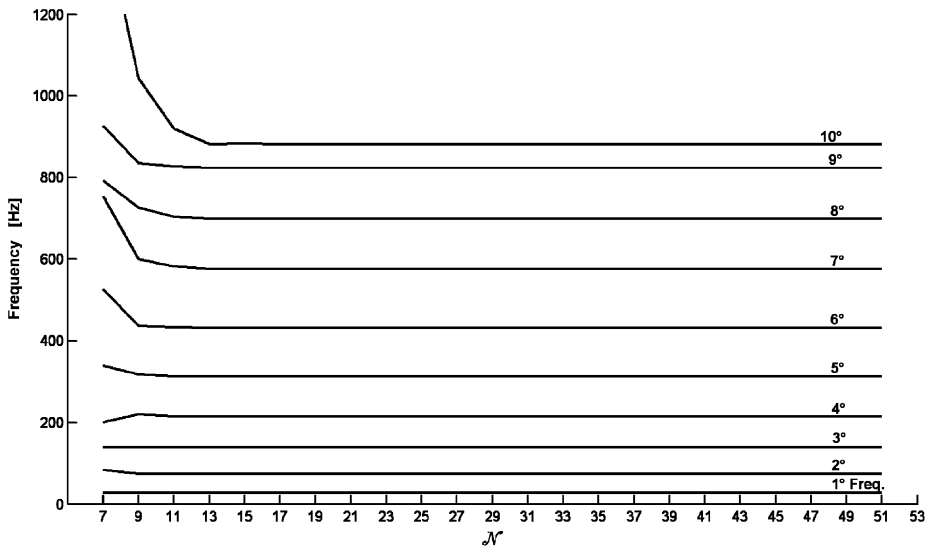

Fig. 4. Convergence and stability characteristics of the first 10 frequencies for multi-stepped hinged–hinged circular arch considered in Table 2.

5. Conclusions

In this paper, two different approaches for the study of free harmonic in-plane vibrations of multi-stepped and multi-damaged circular arches have been presented. The analytical solution is based on the Euler

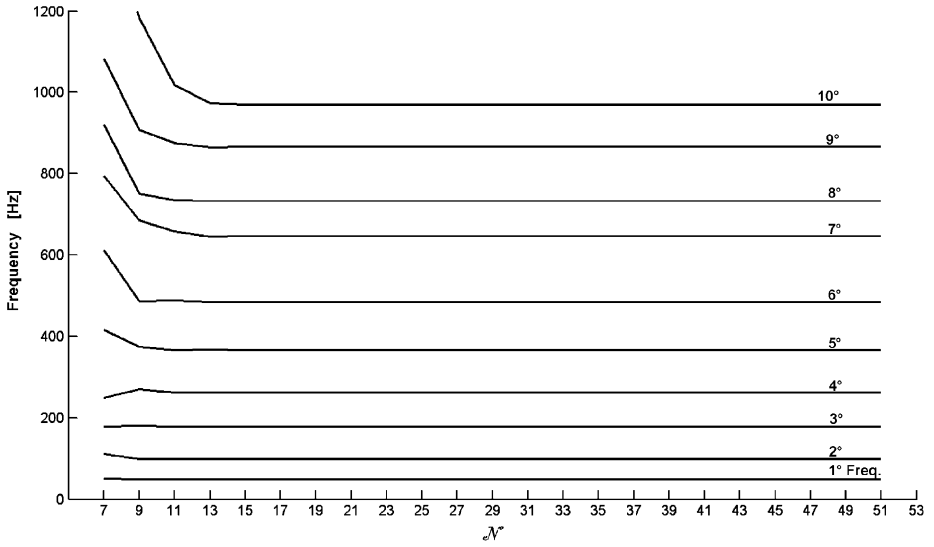

Fig. 5. Convergence and stability characteristics of the first 10 frequencies for multi-stepped clamped–clamped circular arch considered in Table 2.

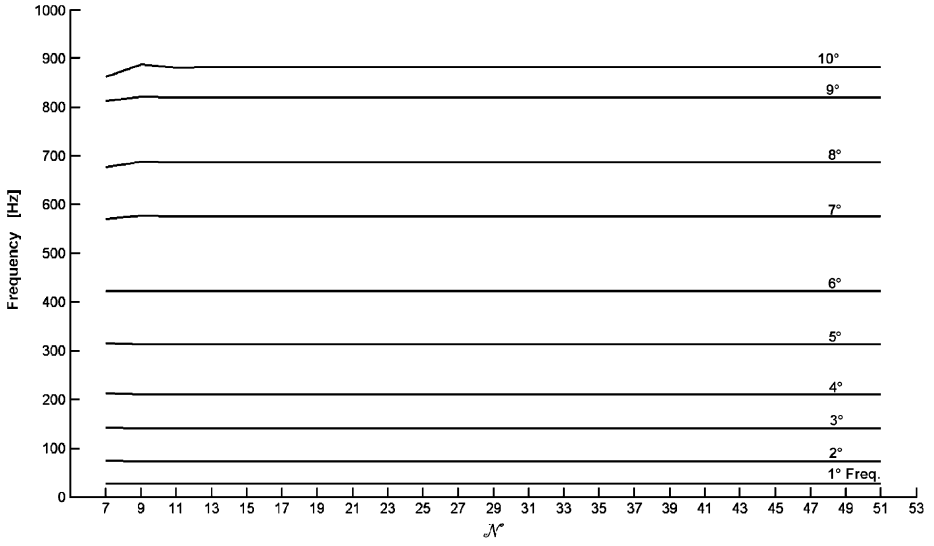

Fig. 6. Convergence and stability characteristics of the first 10 frequencies for multi-stepped hinged–hinged circular arch considered in Table 4.

characteristic exponent procedure involving the roots of characteristic polynomials. On the other hand, the numerical method is focused on the GDQE method. It should be noted that, in the present paper, in deriving the differential equations of motion for each arch portion, equilibrium relations, congruence relations and constitutive relations are combined in a second-order differential equation system considering rotatory inertia, axial extension and transverse shear effects. The solution in terms of radial displacement, tangential displacement and rotation has been derived from the coupled system of three partial differential equations. Multi-stepped arches are considered with different boundary conditions. Several undamaged and damaged configurations have been investigated, modelling the cracked cross-section as an elastic rotational spring. As presented, both methods show to be accurate in predicting natural frequencies, and can be conveniently adopted in localizing a cracked cross-section by modal parameter measures.

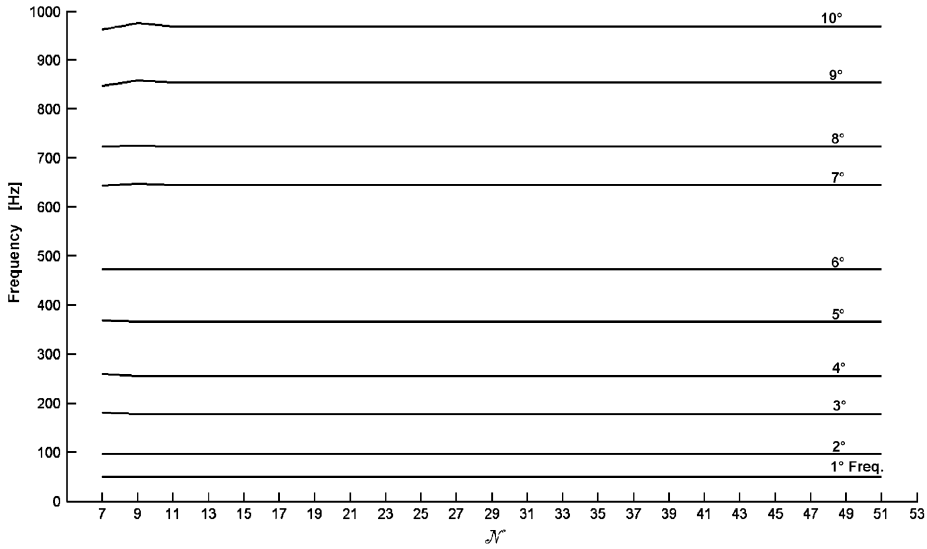

Fig. 7. Convergence and stability characteristics of the first 10 frequencies for multi-stepped clamped–clamped circular arch considered in Table 4.

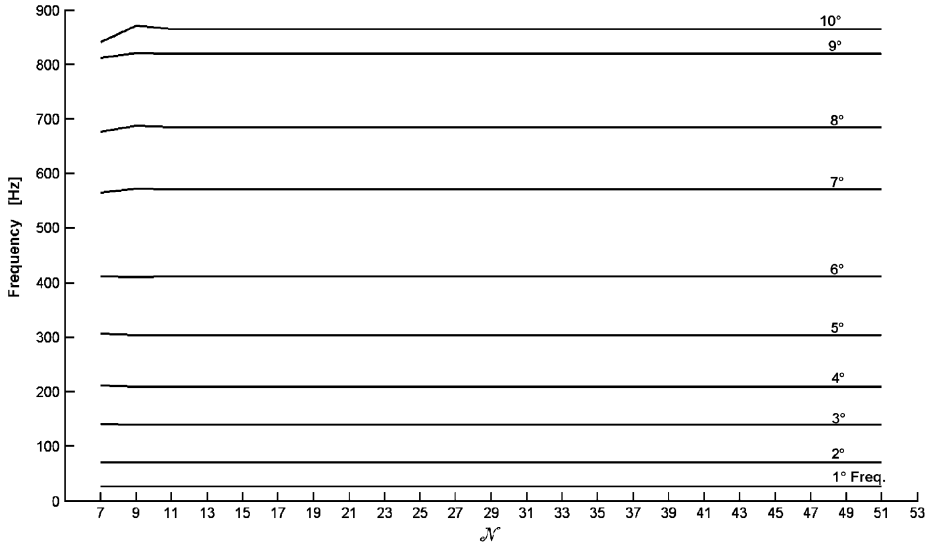

Fig. 8. Convergence and stability characteristics of the first 10 frequencies for multi-stepped hinged–hinged circular arch considered in Table 5.

The GDQE method provides a very simple algebraic formula for determining the weighting coefficients required by the DQ approximation without restricting in any way the choice of mesh grids. Examples presented show that the GDQE method can produce accurate results using only a small number of sampling points. The present method provides converging results for all the cases treated. Fast convergence and very good stability have been shown. Furthermore, discretizing and programming procedures are quite easy.

As far as the dynamic behaviour of structures containing damages is concerned, the topic of damage localization will be discussed briefly. In damage detection problems, two stages have to be taken into account: the localization of the damage and its magnitude or severity. Various objective functions may be considered that account for the difference between analytical and experimental quantities. It is worth noting that modelling and experimental errors will always complicate the problem when trying to reach the exact solution.

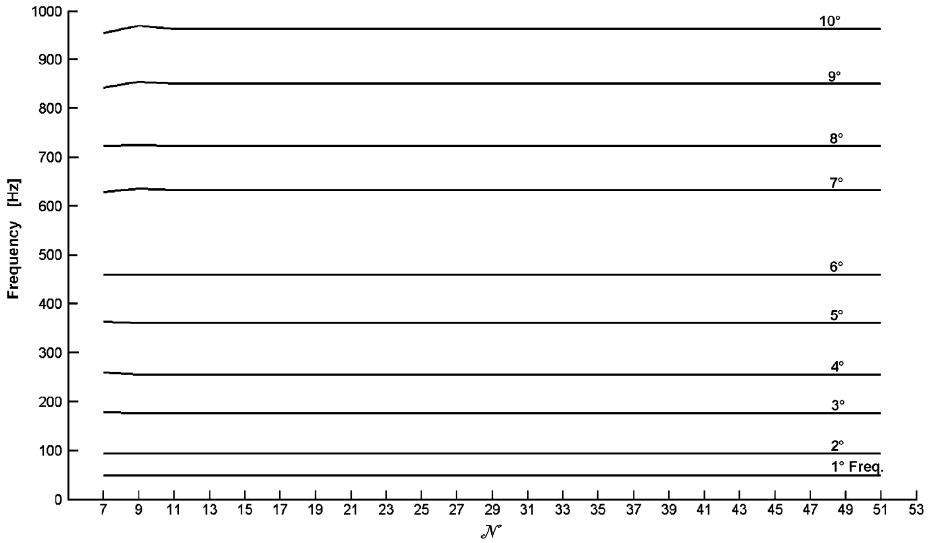

Fig. 9. Convergence and stability characteristics of the first 10 frequencies for multi-stepped clamped–clamped circular arch considered in Table 5.

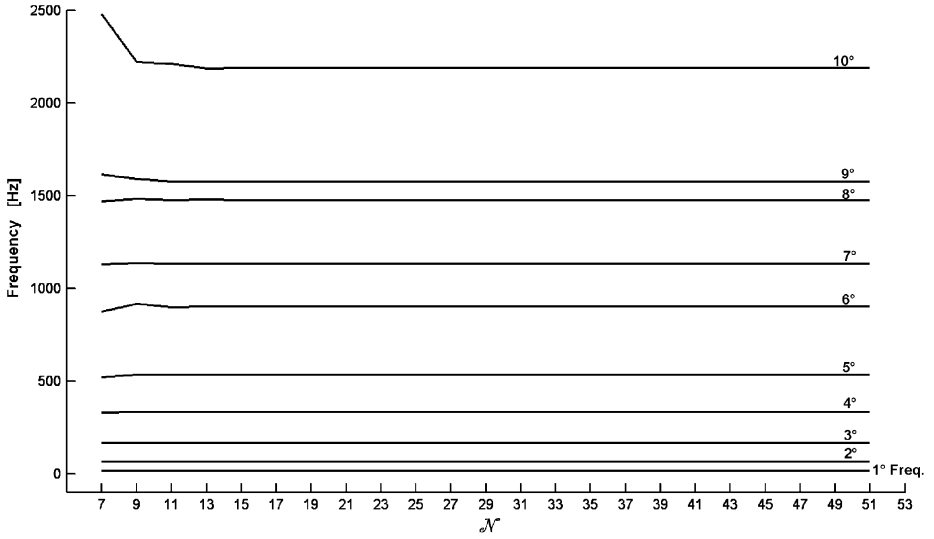

Fig. 10. Convergence and stability characteristics of the first 10 frequencies for multi-stepped clamped–free circular arch considered in Table 7.

The identification procedure is generally based on the minimization of an objective function [35]. Using dynamic methods for damage localization, changes in natural frequency can be considered as the diagnostic tool. Frequencies can be measured more easily than mode shapes and are usually less affected by experimental errors. When experimental data are used, and the numerical model is reliable, the localization of damage can be accurate, though some discrepancies may remain in its quantification, depending on which frequencies are selected from those available. It should be noted that the dynamic techniques have become a viable tool of structural analysis, because of the remarkable progress in the acquisition and treatment of experimental data that have characterized the final decades of the last century.

However, attention has to be addressed to the fact that the identification problems present pathologies and difficulties typical of inverse problems, and this hinders a blind use of the above-mentioned techniques. The presence of non-uniqueness, the lack of stability estimates, etc., make it difficult to do without extra information in analysing the problem of crack localization under discussion. When taking a look at the research activity which has been developed along the years, one is surprised by the huge amount of work done, but one also notices a progressive improvement in the level of awareness of the subtleties involved in this kind of problems [52]. The general properties of identification problems, with specific regard to the sensitivity of natural frequencies to damage, the accuracy of the data, the interpretation model, the determination of "minimal sets" of data needed for the reconstruction of localized damages, should always be studied.

Acknowledgements

This research was supported by the Italian Ministry for University and Scientific, Technological Research MIUR (40% and 60%). The research theme is one of the subjects of the Centre of Study and Research for the Identification of Materials and Structures (CIMEST)—"M. Capurso".

The authors are very grateful to the reviewers for their useful suggestions.

References

[1] J.P. Den Hartog, The lowest natural frequency of circular arcs, *Philosophical Magazine Series 7* 5 (1928) 400–408.
[2] A.E.H. Love, *A Treatise on the Mathematical Theory of the Elasticity*, Dover, New York, 1944.
[3] J.S. Wu, L.K. Chiang, A new approach for free vibration analysis of arches with effects of shear deformation and rotary inertia considered, *Journal of Sound and Vibration* 274 (2004) 49–71.
[4] G. Karami, P. Malekzadeh, In-plane free vibration analysis of circular arches with varying cross-sections using differential quadrature method, *Journal of Sound and Vibration* 274 (2004) 777–799.
[5] E. Viola, E. Artioli, M. Dilena, Analytical and differential quadrature results for vibration analysis of damaged circular arches, *Journal of Sound and Vibration* 288 (2005) 887–906.
[6] K.H. Ng, C.A. Fairfield, Modifying the mechanism method of masonry arches bridge analysis, *Constructions and Building Materials* 18 (2004) 91–97.
[7] M.S. Marefat, E. Ghahremani-Gargary, S. Atei, Load test of a plane concrete arch railway bridge of 20-m span mechanism method of masonry arch bridge analysis, *Constructions and Building Materials* 18 (2004) 661–667.
[8] M. Perty, C.C. Fleischer, Free vibration of a curved beam, *Journal of Sound and Vibration* 18 (1971) 17–30.
[9] K.M. Ahmed, Free vibration of curved sandwich beams by the method of finite elements, *Journal of Sound and Vibration* 18 (1971) 61–74.
[10] G. Prathap, The curved beam/deep arch/finite ring element revisited, *International Journal for Numerical Methods in Engineering* 21 (1985) 389–407.
[11] D.G. Ashwell, R.H. Gallagher, *Finite Element for Thin Shells and Curved Members*, Wiley, London (England), 1976.
[12] C.R. Babu, G. Prathap, A linear thick curved beam element, *International Journal for Numerical Methods in Engineering* 23 (1986) 1313–1328.
[13] R.D. Cook, D.S. Malkus, M.E. Plesha, *Concepts and Applications of Finite Element Analysis*, Wiley, New York, 1989.
[14] D.J. Dawe, Curved finite element for the analysis shallow and deep arches, *Computers & Structures* 4 (1974) 559–580.
[15] D.J. Dawe, Numerical studies using circular arch finite elements, *Computers & Structures* 4 (1974) 729–740.
[16] L.S.D. Morley, Quality of trial functions in quadratic isoparametric representation of an arc, *International Journal for Numerical Methods in Engineering* 19 (1983) 37–47.
[17] A. Tessler, L. Spiridigliozzi, Curved beam elements with penalty relaxation, *International Journal for Numerical Methods in Engineering* 23 (1986) 2245–2262.
[18] H.K. Stolarski, M.Y.M. Chiang, The mode-decomposition, C^0 formulation of curved, two- dimensional structural elements, *International Journal for Numerical Methods in Engineering* 28 (1989) 145–154.
[19] B.D. Reddy, M.B. Volpi, Mixed finite element method for circular arch problem, *Computer Methods in Applied Mechanics and Engineering* 97 (1992) 125–145.
[20] Z. Friedman, J.B. Kosmatka, An accurate two-node finite element for shear deformable curved beams, *International Journal for Numerical Methods in Engineering* 41 (1998) 473–498.
[21] C. Zhang, S. Di, New two-node shear-flexible curved beam elements, *Computational Mechanics* 30 (2003) 81–87.
[22] P. Chidamparam, W. Leissa, Influence of centerline extensibility on the in-plane free vibrations of loaded circular arches, *American Society of Mechanical Engineers* 46 (1993) 467–483.
[23] J. Henrych, *Dynamics of Arches and Frames*, Elsevier, Amsterdam, 1981.
[24] P. Chidamparam, W. Leissa, Influence of centerline extensibility on the in-plane free vibrations of loaded circular arches, *Journal of Sound and Vibration* 183 (1995) 779–795.

[25] X. Tong, N. Mrad, B. Tabarrok, In-plane vibrations of circular arches with variable cross-sections, *Journal of Sound and Vibration* 212 (1988) 121–140.
[26] M.A. De Rosa, C. Franciosi, Exact and approximate dynamic analysis of circular arches using DQM, *International Journal of Solids and Structures* 37 (2000) 1103–1117.
[27] E. Tüfekçi, A. Arpaci, Exact solution of in-plane vibrations of circular arches with account taken of axial extension, transverse shear and rotatory inertia, *Journal of Sound and Vibration* 209 (1998) 845–856.
[28] M.S. Issa, Natural frequencies of continuous curved beams on winkler-type foundation, *Journal of Sound and Vibration* 127 (1988) 291–301.
[29] E. Viola, L. Panzacchi, F. Tornabene, General analysis and application to redundant arches under static loading, *Construction and Building Materials*, 2006, in press. Corrected proof available online 10 February 2006.
[30] M.N. Cerri, G.C. Ruta, Detection of localized damage in plane circular arches by frequency data, *Journal of Sound and Vibration* 270 (2004) 39–59.
[31] M. Krawczuk, W.M. Ostachowicz, Natural vibrations of a clamped–clamped arch with an open transverse crack, *Journal of Vibration and Acoustics* 119 (1997) 145–151.
[32] P.F. Rizos, N. Aspragathos, A.D. Dimarogonas, Identification of crack location and magnitude in a cantilever beam from the vibration modes, *Journal of Sound and Vibration* 138 (1990) 381–388.
[33] W.M. Ostachowicz, M. Krawczuk, Analysis of the effect of a crack on the natural frequencies of a cantilever beam, *Journal of Sound and Vibration* 150 (1991) 191–201.
[34] E. Cabib, L. Freddi, A. Morassi, D. Percivale, Thin notched beams, *Journal of Elasticity* 64 (2001) 157–178.
[35] E. Viola, L. Federici, L. Nobile, Detection of crack location using cracked beam element method for structural analysis, *Theoretical and Applied Fracture Mechanics* 36 (2001) 23–35.
[36] E. Viola, L. Nobile, L. Federici, Formulation of crack beam element method for structural analysis, *ASCE Journal of Engineering Mechanics* 128 (2002) 220–230.
[37] J.A. Loya, L. Rubbio, J. Fernandez-Saez, Natural frequencies for bending vibrations of Timoshenko cracked beams, *Journal of Sound and Vibration* 290 (2006) 640–653.
[38] P. Ricci, E. Viola, Stress intensity factors for cracked T-sections and dynamic behaviour of T-beams, *Engineering Fracture Mechanics* 73 (2006) 91–111.
[39] R. Bellman, J. Casti, Differential quadrature and long-term integration, *Journal of Mathematical Analysis and Application* 34 (1971) 235–238.
[40] R. Bellman, B.G. Kashef, J. Casti, Differential quadrature: a technique for the rapid solution of nonlinear partial differential equations, *Journal of Computational Physics* 10 (1972) 40–52.
[41] K. Kang, C.W. Bert, A.G. Striz, Vibration analysis of shear deformable circular arches by the differential quadrature method, *Journal of Sound and Vibration* 181 (1995) 353–360.
[42] K. Kang, C.W. Bert, A.G. Striz, Vibration and buckling analysis of circular arches using DQM, *Computers & Structures* 60 (1996) 49–57.
[43] C.W. Bert, M. Malik, Differential quadrature method in computational mechanics: a review, *Transactions of the American Society of Mechanical Engineers* 49 (1996) 1–28.
[44] C. Shu, *Differential Quadrature and its Application in Engineering*, Springer, Berlin, 2000.
[45] C.N. Chen, A generalized differential quadrature element method, *Computer Method in Applied Mechanics and Engineering* 188 (2000) 553–556.
[46] G.R. Liu, T.Y. Wu, In-plane vibration analyses of circular arches by the generalized differential quadrature rule, *International Journal of Mechanical Sciences* 43 (2001) 2597–2611.
[47] T.Y. Wu, G.R. Liu, Y.Y. Wang, Application of the generalized differential quadrature rule to initial-boundary-value problems, *Journal of Sound and Vibration* 264 (2003) 883–891.
[48] F. Civan, C.M. Sliepcevich, Differential quadrature for multi-dimensional problems, *Journal of Mathematical Analysis and Application* 101 (1984) 423–443.
[49] F. Civan, C.M. Sliepcevich, Application of differential quadrature in solution of pool boiling in cavities, *Proceeding of Oklahoma Academy of Sciences* 65 (1985) 73–78.
[50] E. Viola, F. Tornabene, Vibration analysis of damaged circular arches with varying cross-section, *Structural Integrity & Durability* 1 (2005) 155–169.
[51] E. Tufekci, O. Ozdemirci, Exact solution of free in-plane vibration of stepped circular arch, *Journal of Sound and Vibration* 295 (2006) 725–738.
[52] C. Davini, E. Viola (Eds.), *Problem in Structural Identification and Diagnostic: General Aspects and Applications*, CISM Courses and Lectures 471, Springer, Wien, New York, 2003.